Intermetallic Compounds

DOI: 10.1002/anie.201203787

Isolated Pd Sites on the Intermetallic PdGa(111) and PdGa($\bar{1}\bar{1}\bar{1}$) Model Catalyst Surfaces**

*Jan Prinz, Roberto Gaspari, Carlo A. Pignedoli, Jochen Vogt, Peter Gille, Marc Armbrüster, Harald Brune, Oliver Gröning, Daniele Passerone, and Roland Widmer**

Catalytic reactions are of highest technological and economic importance, especially in the field of chemical synthesis and exhaust gas treatment.[1] About 80% of the reactions in chemical industry rely on catalysts, thus giving motivation for research in this area.[2,3] There has been enormous progress in heterogeneous catalysis through the understanding of reaction mechanisms and the relation of catalyst surface structures to the reaction rate and selectivity.[3–7] A major step forward has been achieved by comparing single-crystal model catalysts to real catalysts and by combining the ultrahigh-vacuum (UHV) surface-science approach with high-pressure studies of the reaction kinetics.[2–4] This development has led to a paradigm shift in catalyst development.[8]

Amongst the most ingenious and innovative catalyst materials are intermetallic compounds (IMCs) as they enable spatial separation of the catalytically active sites[9] and thus the achievement of both high activity and selectivity.[10] Additionally, it is also possible to tune the electronic properties of IMCs by changing their chemical composition. Recent results revealed that this new class of catalytic materials might be of industrial relevance, and outperform known catalysts, especially when highly selective processes are demanded.[11]

[*] J. Prinz,[+] Dr. R. Gaspari,[+] Dr. C. A. Pignedoli, Dr. O. Gröning, Dr. D. Passerone, Dr. R. Widmer
Empa. Swiss Federal Laboratories for Materials Science and Technology
Überlandstrasse 129, 8600 Dübendorf (Switzerland)
E-mail: roland.widmer@empa.ch
Homepage: http://www.surfaces.ch
Dr. J. Vogt
Chemisches Institut, Otto-von-Guericke-Universität
39106 Magdeburg (Germany)
Prof. Dr. P. Gille
Dept. für Geo- und Umweltwissenschaften
Ludwig-Maximilians-Universität, 80333 München (Germany)
Dr. M. Armbrüster
Max-Planck-Institut für Chemische Physik fester Stoffe
01187 Dresden (Germany)
J. Prinz,[+] Prof. Dr. H. Brune
Institute of Condensed Matter Physics, EPFL, Station 3
1015 Lausanne (Switzerland)
[+] These authors contributed equally to this work.

[**] This work was supported by the Swiss National Science Foundation under the contract 200021-129511. We kindly acknowledge D. Rosenthal, R. Schlögl (FHI Berlin), and Y. Grin (MPI Dresden) for fruitful discussions, and the Swiss Supercomputing Center (CSCS) for computational resources.

Supporting information for this article is available on the WWW under http://dx.doi.org/10.1002/anie.201203787.

PdGa IMCs have shown remarkable catalytic properties for an important reaction in polyethylene production, namely the partial hydrogenation of acetylene to ethylene.[11,13–15] However, the reaction pathway is largely unknown. We address this question on single-crystal IMC PdGa model systems.[4] Their bulk crystal and electronic structure have been reported earlier.[11–14,16–18] Herein, we determine and explore the stable surface terminations because they define the activity and selectivity of the catalyst.[8]

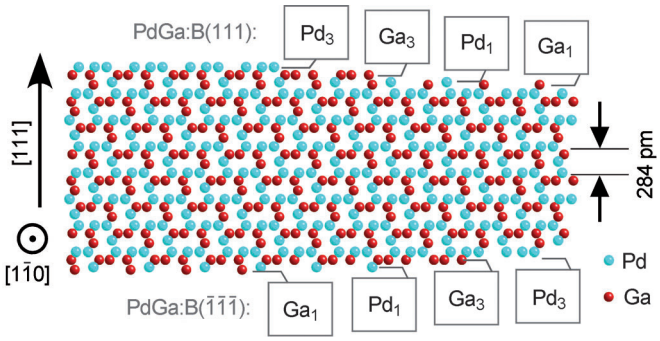

Figure 1. Bulk-truncated surface terminations of the PdGa:B(111) and ($\bar{1}\bar{1}\bar{1}$) surfaces. The surfaces are named according to Ref. [12], including the chemical composition, the enantiomeric form, and the surface direction.

We combine quantitative low-energy electron diffraction (LEED), high-resolution scanning tunneling microscopy (STM), and ab initio thermodynamics calculations to unequivocally identify the surface terminations of PdGa(111) and PdGa($\bar{1}\bar{1}\bar{1}$) surfaces. These surfaces exhibit significant differences in catalytic activity that are exemplified by calculations of hydrogen dissociation.

The crystal structure of PdGa belongs to the $P2_13$ space group and therefore exhibits two enantiomeric forms (labeled A and B in Refs. [12,19]). Figure 1 displays a side view onto a (1$\bar{1}$0) surface of the structure model of form B that was derived from X-ray diffraction.[16] The stacking sequence involves four nonequivalent atomic planes. As a consequence, the top and bottom surfaces are different, and each can exhibit four possible terminations. Recent STM investigations[12] revealed that there is only one step height, and its value of 284 pm corresponds to four atomic planes, thus implying that only one of the four terminations is realized. LEED and X-ray photoelectron diffraction have shown that the surfaces are chiral and unreconstructed.[12] Herein, we identify which of the four bulk terminations is realized and discuss the structure–reactivity relation.

Our initial approach to determining the surface terminations was by using LEED. This technique is intrinsically surface sensitive because of the small mean-free path of low-energy electrons. In addition to the diffraction images of the surface unit cells, information on the vertical structure was acquired from the variation of the diffraction spot intensities with incident electron energy owing to the interference of electrons scattered from lower-lying layers. Comparison of these *I–V* curves with simulated ones allows the determination of the atomic positions of the first atomic layers. The quality of this comparison is quantified by the Pendry reliability factor R_P[20] which is 0 for perfect agreement and 1 for uncorrelated profiles. The agreement is acceptable when R_P is less than 0.3.[20,21]

We compared experimental results to the theoretical results for the 32 possible structures that result from both enantiomeric forms of the crystal, the four bulk truncations, the two nonequivalent close-packed surfaces, that is, (111) and $(\bar{1}\bar{1}\bar{1})$, and both possible in-plane orientations of the sample. Density functional theory (DFT) was used to compute the atomic positions of the relaxed bulk-surface terminations. The SATLEED code was applied to calculate the LEED curves from these model structures.[21,22] The atomic positions were further fine-tuned to minimize the R_P factor for a given termination. The R_P factors for the model structures that were closest to the experimental structures are presented in Figure 2. The best fit was found for the PdGa:B(111)Pd_3 and PdGa:B$(\bar{1}\bar{1}\bar{1})Pd_1$ surface structures of the respective samples.

The difference in the R_P factor between the proposed structures is larger for the (111) surface than for the $(\bar{1}\bar{1}\bar{1})$ surface because of the much lower atomic density of the latter, and the weaker scattering cross section when Pd_1 terminated. Nevertheless, the difference remains significant also in that case, and the best fit for both structures give $R_p = 0.22$. To get an impression of the agreement between experimental and theoretical results, in Figure 2 we show for each surface the *I–V* curves for the structures with the lowest and highest R_p factors. Notably, the atomic displacements from the DFT relaxed structure that was used for the

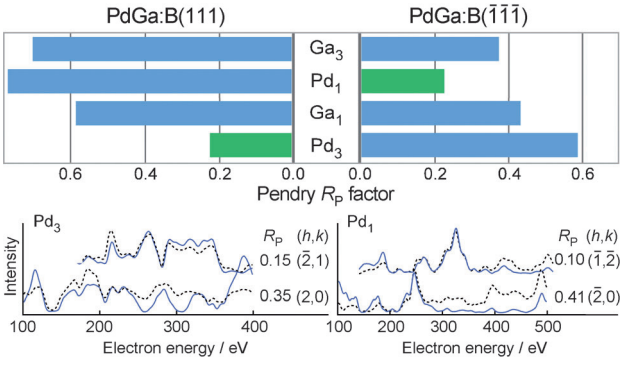

Figure 2. Top: R_P factors for the surface terminations that are shown in Figure 1. The experimental *I–V* data is derived from an average of 12 nonequivalent diffraction spots for each sample. The terminations giving best agreement are marked in green. Bottom: Experimental (dashed black line) and theoretical *I–V* curves (full blue line) for the two spot profiles that are in best and worst agreement among those of Pd_3 and Pd_1 (see also the Supporting Information).

optimization of the R_p factor are very small, being less than 7 pm in the vertical and less than 27 pm in the lateral direction. Finally, our LEED patterns confirm the formerly found absence of a surface reconstruction.[12]

The surface terminations found by LEED are confirmed by the atomic resolution STM images shown in Figure 3. The unit cells are imaged as a trimer for the (111) surface and as a single atomic protrusion for the $(\bar{1}\bar{1}\bar{1})$ surface. In both cases,

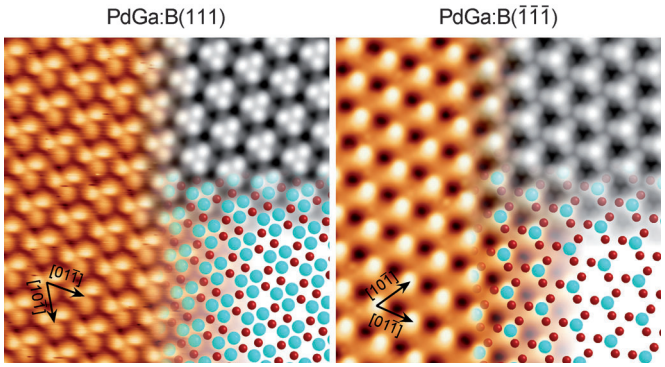

Figure 3. Atomically resolved STM images ($T = 77$ K) overlaid with simulated STM images (top right inset) and the respective structure models (bottom right inset; Pd = aqua, Ga = red). STM parameters (PdGa:B(111)Pd_3)/(PdGa:B$(\bar{1}\bar{1}\bar{1})Pd_1$): $V_T = 80/100$ mV; $I_T = 0.73/0.4$ nA; $\Delta z = 32/51$ pm; scan size = 6×6 nm^2.

the periodicity corresponds to the bulk value of 0.693 nm.[16] This atomic contrast was found for all terraces of the respective surfaces, thus confirming that only one stable termination exists. The STM simulations shown in the top right insets agree with the experimental results. These simulations were obtained by applying the Tersoff-Hamann (TH) formalism[23] to the DFT computed local density of states (LDOS; see the Supporting Information), the isovalue of which is matched to give good agreement with the experiment.

We addressed the physical origin of the stability of the identified terminations with DFT calculations. The relative stability of all PdGa terminations were computed in the grand canonical ensemble, where the different surfaces are at equilibrium with external sources of Pd and Ga atoms, and the equilibrium state is determined by the minimum of the Gibbs surface energy, G_s. The chemical potentials of the Pd and Ga atoms, μ_{Pd} and μ_{Ga}, depend on external parameters, such as pressure and temperature, and their individual values are generally unknown. However, the range of allowed μ_{Pd} and μ_{Ga} values can be determined by thermodynamic considerations.[24] The upper limit of the chemical potential of Pd and Ga in the alloy is given by the respective bulk values. Moreover, when the sources of Pd and Ga atoms are in equilibrium with the PdGa bulk, μ_{PdGa} is a function of μ_{Pd} and μ_{Ga}. This gives an interval of [Eq. 1]:

$$\mu_{Ga}^{bulk} + \frac{\Delta H_f}{4} \le \mu_{Ga} \le \mu_{Ga}^{bulk}$$
$$\mu_{Pd}^{bulk} + \frac{\Delta H_f}{4} \le \mu_{Pd} \le \mu_{Pd}^{bulk} \quad (1)$$

where ΔH_f is the enthalpy of formation of PdGa per unit cell, containing four Pd and four Ga atoms. For the bulk cohesive energies we find $\mu_{Pd}^{bulk} = -3.69$ eV and $\mu_{Ga}^{bulk} = -2.78$ eV, which are in agreement with previous results.[25,26] For the heat of formation per PdGa unit cell we obtain $\Delta H_f = -5.48$ eV, which is close to the experimental value of -5.96 eV.[27]

For both surface orientations, Figure 4 displays the resulting $\Delta G_s(\mu_{Ga})$ curves, computed using periodic slab calculations.[28] ΔG_s is expressed relative to PdGa:B(111)Ga_3

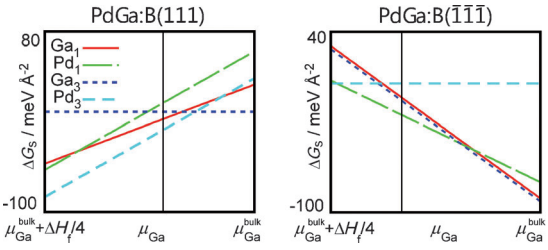

Figure 4. Change in Gibbs surface energy as a function of μ_{Ga} for the different terminations. Vertical lines refer to the actual value of the surface chemical potential estimated for the respective PdGa surfaces.

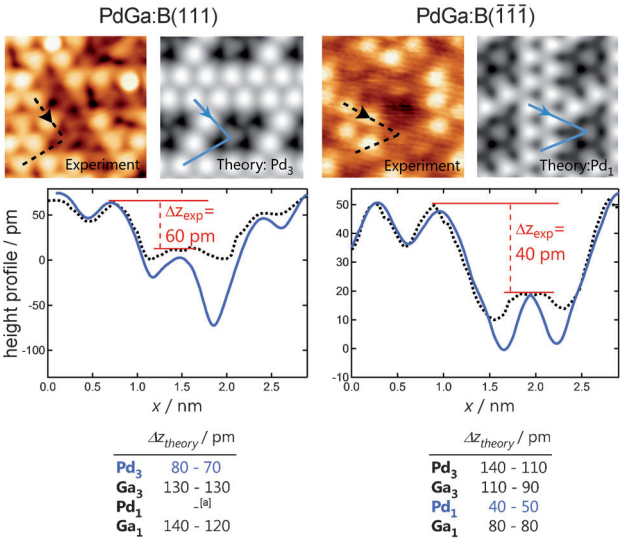

Figure 5. Top: Measured and calculated constant-current STM images. Middle: Apparent height profiles for experimental (dashed black line) and simulated (full blue line) STM images of surface vacancies. Bottom: The tables show simulated values of the apparent vacancy depths (Δz) for all DFT relaxed model terminations. The values that have best agreement between simulation and experiment are marked in blue. [a] In the DFT-optimized structure for (111)Pd_1 the underlying Ga layer relaxes towards the surface and becomes the top layer.

and PdGa:B$(\bar{1}\bar{1}\bar{1})Pd_3$, respectively (see the Supporting Information). The graphs shown reveal which surfaces can be expected over the whole range of external parameters. Clearly, the surface terminations determined by experiment have the widest stability ranges with a $\Delta\mu_{Ga}$ value of 1 eV and 0.8 eV in the two cases. This finding confirms the experimental results for both surfaces. Moreover, the actual values of the chemical potentials can be estimated under the assumptions that the Pd and Ga sources are in equilibrium with kink sites of the crystal surface and that the two opposite surfaces of the same sample equilibrate independently. The explicit calculation (see the Supporting Information) gives values of $\mu_{Ga}^{(111)} = \mu_{Ga}^{bulk} - 0.57$ eV and $\mu_{Ga}^{(\bar{1}\bar{1}\bar{1})} = \mu_{Ga}^{bulk} - 0.90$ eV, which are indicated in the energy profiles (Figure 4) as vertical lines. Again, for these specific values $Pd_3(111)$ and $Pd_1(\bar{1}\bar{1}\bar{1})$ are found to be the most stable terminations, in agreement with the experimental results.

STM images of surface vacancies provide an additional and very sensitive test of the determined surface terminations. The distance from the surface as well as the chemical composition of the underlying layer varies strongly with the surface termination, thus giving rise to termination specific STM contrast between the surface and vacancies. Figure 5 shows a comparison of measured and calculated constant-current STM images and apparent height profiles going from regular surface areas to vacancies and back. The surface layer is identified from the simulated STM vacancy profiles for all bulk terminations, by comparison of the calculated vacancy depths with the experimental value.

For both surfaces, the measured apparent-vacancy heights agree well with the calculated ones for the two identified terminations, and differ significantly from all other terminations. This result gives us additional confidence that PdGa:B(111)Pd_3 and PdGa:B$(\bar{1}\bar{1}\bar{1})Pd_1$ are the actual surface structures. The STM simulations were obtained using the TH[23] model and DFT relaxed surface structures displaying patterns of 2×2 vacancies with monoatomic steps. The comparison of experimental and theoretical results is particularly robust, as the vacancy depth is rather stable against changes of simulated isocurrent or tip radius. A large range of tip–sample distances was covered by simulating STM images for integrated LDOS values of 10^{-7} and 10^{-11} e Å^3. For a pointlike tip, these values correspond to tip–sample distances of 0.45 nm and 0.9 nm, respectively. The vacancy depth intervals given in Figure 5 come from these two extreme tip–sample distances and provide a conservative error margin of the STM simulation.

An initial indication of the catalytic activity of the two surface terminations can be obtained from the position of the metal d-band center with respect to E_F, an indicator for the bonding strength of adsorbates to metallic surfaces.[29] However, this simple d-band-center rule has to be taken with care, both, because covalent bonding plays a role in this system, and in case molecular adsorption modifies considerably the band shape (as seen in the Supporting Information, this is the case for hydrogen adsorption).[30] For high catalytic activity, the bond to a reactant molecule should be of intermediate strength, this is known as the Sabatier principle.[31] In comparison to Pd(111), (for details see the Supporting Information) the Pd d-band edge of both PdGa surfaces is found at lower energy, which is an indication (with the above caveats) of a weaker binding of the adsorbed molecules on the IMC surfaces, in agreement with thermal desorption spectroscopy (TDS) results.[12] Additionally, the PdGa surfaces exhibit a sharper d-band, and thus a stronger localization of electronic states. In spite of their electronic similarity, as seen

by the projected density of states (pDOS; see the Supporting Information), the two PdGa terminations allow for different adsorption conformations as single Pd atoms or Pd trimers terminate the surface. This site separation is particularly evident for Pd_1, where the surface atomic Pd–Pd distance is 2.5 times larger than for Pd(111), and more than twice the bulk value of PdGa.[14]

A more elaborate assessment of the catalytic properties can be obtained by DFT calculations of the binding energies and adsorption sites; we performed these calculations for molecular and atomic hydrogen adsorbed onto both surfaces (Figure 6) while no hydrogen uptake into the bulk is expected.[32] On PdGa:B$(\bar{1}\bar{1}\bar{1})$Pd$_1$ the most favorable adsorption site for H_2 is the Pd_1 on-top position with an adsorption energy of 0.22 eV per H_2 molecule. From this site H_2 dissociation is exothermic with 0.11 eV and the most favorable site for atomic hydrogen is the threefold coordinated hollow site on the Pd_3 trimer (Figure 6, right). This position is 70 pm below the Pd_1 surface plane, and 13 pm below the first Ga_3 plane, a site that is sufficiently close to the surface for the adsorbate to remain available for the hydrogenation of other molecules.

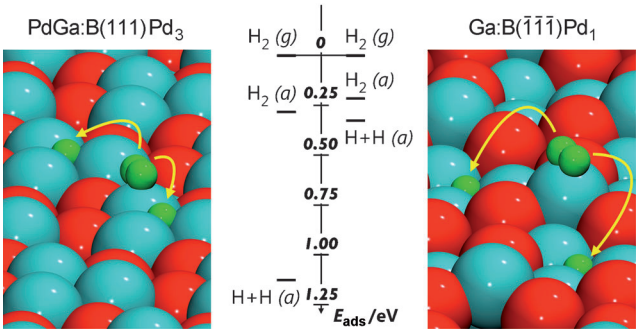

Figure 6. Adsorption sites and binding energies for H_2 and H on the investigated surfaces. Energies are given in eV per H atom couple with respect to the molecule in the gas phase.

The adsorption energy of H_2 on PdGa:B(111)Pd$_3$ is 0.28 eV, and thus comparable to PdGa:B$(\bar{1}\bar{1}\bar{1})$Pd$_1$. Furthermore, similar adsorption positions for H_2 and H are identified for both surfaces, that is, Pd top site and Pd threefold hollow site, respectively. However, H_2 dissociation is associated with a larger energy gain of 0.85 eV on the Pd_3 termination. This comparison reveals that both surface orientations with their terminations determined in the present study show mostly quantitative differences in their behavior towards H_2 dissociation. Although the binding energies of the molecular precursor are quite similar, one surface has more strongly bound dissociation products than the other. The different bonding mechanisms of both surfaces are also highlighted by the projected densities of states. Hybridization of the H s level with the Pd d bands shows a different fine structure at around 6 eV below the Fermi energy (see the Supporting Information), which is where there is maximum overlap between H and Pd orbitals participating in the bonding (as it results from a bond-order analysis performed within Bader's topological theory of atoms in molecules,[33] see Supporting Information. This analysis also confirms the stronger bonding of H atoms on the surface trimer on the PdGa:B(111)Pd$_3$).

In conclusion, we have determined the surface terminations of the IMC PdGa:B(111)Pd$_3$ and PdGa:B$(\bar{1}\bar{1}\bar{1})$Pd$_1$. The structural details revealed in this work and their implications on the binding of adsorbates will serve as the essential basis for understanding chemical reactions on the PdGa surfaces and help develop high performance catalysts from intermetallic compounds. The structural dissimilarities of the two surface terminations lead to significant energetic differences in the catalytic dissociation of a molecule as simple as hydrogen, an essential reagent in many relevant reactions. We expect similar or even larger differences for organic molecules, a topic to be addressed in a forthcoming publication. Moreover, the structural dissimilarity of the (111) and $(\bar{1}\bar{1}\bar{1})$ surfaces makes the IMC PdGa a prototype model system, which allows the study of the effect of active-site separation in heterogeneous catalysis.

Experimental Section

Methods: The single-crystal samples used in this study originate from one large PdGa crystal grown by the Czochralski method.[34] After cutting and polishing, reflective energy dispersive X-ray diffraction determined the surface orientations to be within 0.3° precise.

STM measurements were performed with an Omicron low-temperature STM at 77 K and at a base pressure below 5×10^{-11} mbar with a mechanically cut Pt/Ir-tip. STM data were analyzed using the WSxM software.[35]

Sample preparation in UHV consists of several sputter-annealing cycles (sputtering: Ar^+, 1 keV; annealing: 20 min at 870 K) until a sharp (1×1) LEED pattern was obtained. During preparation, no change in the surface stoichiometry of PdGa was observed.[12] The LEED investigations were carried out with an Omicron multichannelplate Specta-LEED and acquired with a CCD camera at 1 eV/frame. Video analysis was performed using the Spectaview software from Omicron. *I–V* profiles for the single spots were background corrected. The angle of incidence was perpendicular to the surface, thus allowing for averaging over the symmetry equivalent spot profiles leading to an improved signal to noise ratio.[21–22]

Relative surface energies have been computed using DFT slab calculations, employing the PWSCF[36] code. Simulated STM vacancy heights have been computed using supercell DFT slab calculations employing the CP2K[37] code (for further details see the Supporting Information).

Received: May 16, 2012
Revised: June 8, 2012
Published online: August 22, 2012

Keywords: density functional calculations · electron diffraction · heterogeneous catalysis · intermetallic compounds · surface chemistry

[1] U. Dingerdissen, A. Martin, D. Herein, H. J. Wernicke in *Handbook of Heterogeneous Catalysis* (Eds.: G. Ertl, H. Knözinger, F. Schüth, J. Weitkamp), VCH, Weinheim, **2008**.
[2] J. A. Dumesic, G. W. Huber, M. Boudart in *Handbook of Heterogeneous Catalysis* (Eds.: G. Ertl, H. Knözinger, F. Schüth, J. Weitkamp), VHC, Weinheim, **2008**.

[3] G. Kyriakou, M. B. Boucher, A. D. Jewell, E. A. Lewis, T. J. Lawton, A. E. Baber, H. L. Tierney, M. Flytzani-Stephanopoulos, E. C. H. Sykes, *Science* **2012**, *335*, 1209 – 1212.
[4] G. A. Somorjai, *Science* **1985**, *227*, 902 – 908.
[5] H. J. Freund, N. Ernst, T. Risse, H. Hamann, G. Rupprechter, *Phys. Status Solidi A* **2001**, *187*, 257 – 274.
[6] G. Ertl, H. J. Freund, *Phys. Today* **1999**, *52*, 32 – 38.
[7] M. Ortega Lorenzo, C. J. Baddeley, C. Muryn, R. Raval, *Nature* **2000**, *404*, 376 – 379.
[8] J. K. Nørskov, T. Bligaard, J. Rossmeisl, C. H. Christensen, *Nat. Chem.* **2009**, *1*, 37 – 46.
[9] W. M. H. Sachtler, *Catal. Rev. Sci. Eng.* **1976**, *14*, 193 – 210.
[10] M. Armbrüster in *Encyclopedia of Catalysis* (Ed.: I. T. Horvath), VCH, Weinheim, **2011**.
[11] J. Osswald, K. Kovnir, M. Armbrüster, R. Giedigleit, R. E. Jentoft, U. Wild, Y. Grin, R. Schlögl, *J. Catal.* **2008**, *258*, 219 – 227.
[12] D. Rosenthal, R. Widmer, R. Wagner, P. Gille, M. Armbrüster, Y. Grin, R. Schlögl, O. Gröning, *Langmuir* **2012**, *28*, 6848 – 6856.
[13] J. Osswald, R. Giedigkeit, R. E. Jentoft, M. Armbrüster, F. Girgsdies, K. Kovnir, T. Ressler, Y. Grin, R. Schlögl, *J. Catal.* **2008**, *258*, 210 – 218.
[14] K. Kovnir, M. Armbrüster, D. Teschner, T. V. Venkov, F. C. Jentoft, A. Knop-Gericke, Y. Grin, R. Schlögl, *Sci. Technol. Adv. Mater.* **2007**, *8*, 420 – 427.
[15] M. Armbrüster, K. Kovnir, M. Behrens, D. Teschner, Y. Grin, R. Schlögl, *J. Am. Chem. Soc.* **2010**, *132*, 14745 – 14747.
[16] M. Armbrüster, H. Borrmann, M. Wedel, Y. Prots, R. Giedigkeit, P. Gille, *Z. Kristallogr. New Cryst. Struct.* **2010**, *225*, 617 – 618 (please consider the accidental interchanging of crystal form "A" and "B" in this reference).
[17] B. H. Verbeek, P. K. Larsen, W. M. Gerits, *Vacuum* **1983**, *33*, 813 – 814.
[18] K. Kovnir, M. Armbrüster, D. Teschner, T. V. Venkov, L. Szentmiklosi, F. C. Jentoft, A. Knop-Gericke, Y. Grin, R. Schlögl, *Surf. Sci.* **2009**, *603*, 1784 – 1792.
[19] J. C. H. Spence, J. M. Zuo, M. Okeeffe, K. Marthinsen, R. Hoier, *Acta Crystallogr. Sect. A* **1994**, *50*, 647 – 650.
[20] J. B. Pendry, *J. Phys. C* **1980**, *13*, 937 – 944.
[21] M. A. Van Hove, W. H. Weinberg, C. M. Chan, *Low-Energy Electron Diffraction*, Springer, Heidelberg, **1986**.
[22] A. Barbieri, M. A. Van Hove, private communication (http://www.ap.cityu.edu.hk/personal-website/Van-Hove.htm) ed.
[23] J. Tersoff, D. R. Hamann, *Phys. Rev. B: Condens. Matter Mater. Phys.* **1985**, *31*, 805 – 813.
[24] G. X. Qian, R. M. Martin, D. J. Chadi, *Phys. Rev. B: Condens. Matter Mater. Phys.* **1988**, *38*, 7649 – 7663.
[25] D. D. Wagman, W. H. Evans, V. B. Parker, R. H. Schumm, I. Halow, S. M. Bailey, K. L. Churney, R. L. Nuttall, *J. Phys. Chem. Ref. Data* **1982**, *11*, 1 – 405.
[26] C. Kittel, *Introduction to Solid State Physics*, Wiley, New York, **1971**.
[27] S. V. Meschel, O. J. Kleppa, *Thermochim. Acta* **1997**, *292*, 13 – 17.
[28] W. E. Pickett, *Comput. Phys. Rep.* **1989**, *9*, 115 – 197.
[29] B. Hammer, J. K. Norskov, *Surf. Sci.* **1995**, *343*, 211 – 220.
[30] A. Roudgar, A. Gross, *J. Electroanal. Chem.* **2003**, *548*, 121 – 130.
[31] P. Sabatier, *Ber. Dtsch. Chem. Ges.* **1911**, *44*, 1984 – 2001.
[32] M. Klanjsek, et al., *J. Phys.: Condens. Matter* **2012**, *24*, 085703.
[33] J. G. Angyan, M. Loos, I. Mayer, *J. Phys. Chem.* **1994**, *98*, 5244 – 5248.
[34] P. Gille, T. Ziemer, M. Schmidt, K. Kovnir, U. Burkhardt, M. Armbrüster, *Intermetallics* **2010**, *18*, 1663 – 1668.
[35] I. Horcas, R. Fernandez, J. M. Gomez-Rodriguez, J. Colchero, J. Gomez-Herrero, A. M. Baro, *Rev. Sci. Instrum.* **2007**, *78*, 013705.
[36] P. Giannozzi, et al., *J. Phys.: Condens. Matter* **2009**, *21*, 395502.
[37] J. VandeVondele, M. Krack, F. Mohamed, M. Parrinello, T. Chassaing, J. Hutter, *Comput. Phys. Commun.* **2005**, *167*, 103 – 128.

Angewandte Chemie
Eine Zeitschrift der Gesellschaft Deutscher Chemiker

Supporting Information

69451 Weinheim, Germany

Isolated Pd Sites on the Intermetallic PdGa(111) and PdGa($\bar{1}\bar{1}\bar{1}$) Model Catalyst Surfaces**

*Jan Prinz, Roberto Gaspari, Carlo A. Pignedoli, Jochen Vogt, Peter Gille, Marc Armbrüster, Harald Brune, Oliver Gröning, Daniele Passerone, and Roland Widmer**

anie_201203787_sm_miscellaneous_information.pdf

Supporting Information (SI)

Table of Contents

1. LEED-I(V) calculation part:

In the first step of simulating the I(V) profiles, the potential landscape within the material is approximated as a muffin-tin potential, where the individual atomic cores are assumed to form symmetric spherical potentials with the muffin-tin radius, embedded in a region of constant potential, the "muffin-tin zero", or "inner potential". For the PdGa structure, the radii of the respective atoms were chosen as half the distance to the nearest neighbor. By solving the Schrödinger equation for an electron scattered on an individual atom, i.e. a certain spherical potential, the energy dependent phase shifts for the scattering process were obtained. For these calculations, the phase shift package of Barbieri and Van Hove[1] was used.

The next steps are the calculations of the intensity vs. energy profiles for different reference model structures and the optimization of the atomic coordinates via comparison to the experiment. For this, the reliability factor R_P was used, as defined by Pendry.[2] A value of $R_P = 0$ would result from a perfect correlation of experiment and theory, whereas $R_P = 1$ means uncorrelated profiles. If $R_P < 0.3$ the agreement is considered to be acceptable. The SATLEED code used throughout this study makes use of the tensor LEED approximation.[3-4] Within tensor LEED, the time consuming solution of the multiscattering problem in LEED is limited to the reference structure only, while the I(V) profiles of a large number of test structures deviating moderately from this reference structure are calculated efficiently by means of a perturbation treatment.

In the main article, we present only the comparisons for structure models of the enantiomer form B, the correct sample in-plane rotation (explained later in the text) and the surface directions according to the respective sample ((111) and (-1-1-1)). However, during the analysis, a total of 32 sets of profiles originating from 32 model structures were compared to both sets of I(V) profile, for the (111) and the (-1-1-1) surface. This number arises from 4 different layers in the surface unit cell (Pd_3, Ga_3, Pd_1, Ga_1), 2 non-equivalent surfaces ((111) and (-1-1-1)), 2 enantiomeric forms and 2 possible rotational directions of the sample in the LEED setup. The latter originates from the unknown in-plane direction of the 3-fold symmetric sample. This problem is equal to the question of how to assign Miller's indices to the experimental spots for the hexagonal pattern with a 3-fold rotational symmetry. A summary of the R-factors is shown as a barchart in Figure 7.

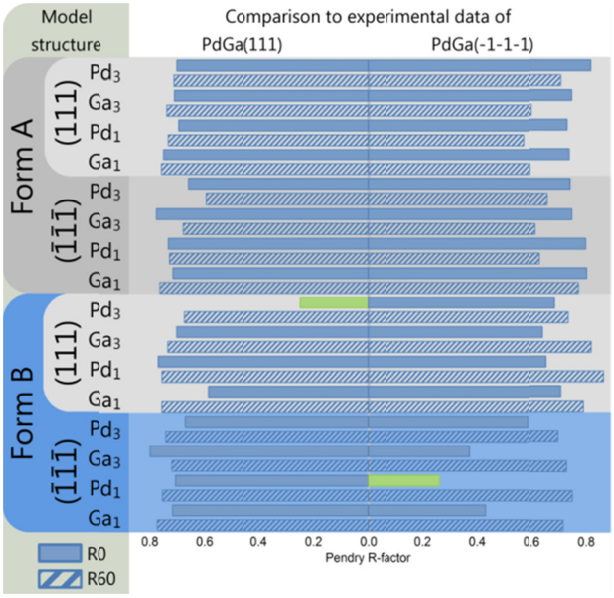

Figure 7 R_P factors from the comparison of all structure models taken into account in the comparison of experimental and theoretical I(V) profiles. For each surface termination, two possible rotations of the surface had to be considered (R0 and R60).

The R_p values shown in Figure 3 and 7 were obtained after fitting out-of-plane and in-plane lattice parameters of the top 9-12 atomic layers, depending on the respective structure model, and the real part of the inner potential.[5] Calculations for obtaining the R_p factors presented in Figure 7 were carried out using a low maximum angular momentum (L_{max} = 6) in the simulated scattering process to increase convergence stability. For the precise determination of the atomic arrangement, the computation was optimized for the two identified structures using L_{max} = 8 and a repetitive optimization of the model structure, using the previous best-fit structure as a new reference structure.[5] Starting from the DFT relaxed structure models, this optimization procedure involved shifts of the atoms from their initial positions not larger than 7 pm in the direction perpendicular to the surface with respect to the lowest layer of the fitted stack. The in-plane shifts of the structure optimization were less than 27 pm.

Resulting I(V) profiles are shown in Figure 8 and in the lower part of Figure 3.

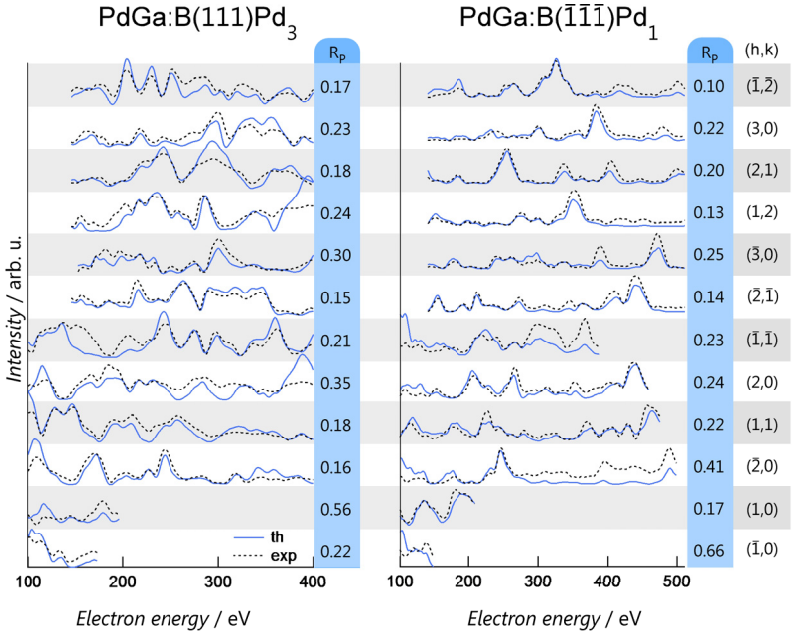

Figure 8 Experimental (dashed) and theoretical I(V) profiles (drawn, blue) for the best fits showing visual agreement for both surfaces. To the right of each profile, the respective spot indices (h,k) and the individual R_p is given. The overall R_p are 0.22 for both surfaces.

The model structures consisted of two, so called composite layers[5]: a substrate part of 12 layers, where the atoms were kept fixed and the coordinates were determined by DFT bulk relaxation and on top of this, a surface part, composed of 9 to 12 layers, depending on the surface model. Here, the initial atomic structure was taken from the DFT relaxation described later. In general, the error bars determined according to Pendry[2] are larger than the actual shift, meaning that the precision of the initial DFT relaxed structure was already good.

2. Surface energy calculation part:

PdGa surface stability was calculated in the framework of periodic slab simulations. For all the slabs considered, the unit cell is primitive along the surface plane. In the direction perpendicular to the surface, 20 Å of vacuum have been added in order to decouple the two surfaces of the slab (see Figure 9). We prepared two stoichiometric slabs of 24 layers (two bulk units) and 36 layers (three bulk units), respectively, both terminated (111)Ga_3 and (-1-1-1)Pd_3. We computed the bulk energy of PdGa as the energy difference of the two relaxed slabs, following the prescription of Ref. [6-7]. By adding layers on the (111)Ga_3/(-1-1-1)Pd_3 slab (24 layers), according to the stacking sequence, we obtained the (111)X/(-1-1-1)Pd_3, (111)Ga_3/(-1-1-1)X slabs, X being any of the 4 bulk terminations (Ga_1, Ga_3, Pd_1, Pd_3). In the (111) direction the 0K DFT energy of each slab, $E_{slab}^{(111)X,\,(-1-1-1)Pd3}$ is approximately related to the surface energies $G^{(111)X}(\mu_{Ga})$ and $G^{(-1-1-1)Pd3}(\mu_{Ga})$ by the relationship

$$G_{surf}^{(111)X}(\mu_{Ga}) + G_{surf}^{(-1-1-1)Pd3}(\mu_{Ga}) \approx E_{slab}^{(111)X/(-1-1-1)Pd3} - (n_{Pd}^{(111)X/(-1-1-1)Pd3}\mu_{Pd} + n_{Ga}^{(111)X/(-1-1-1)Pd3}\mu_{Ga})$$

Equation 1

n_{pd} and n_{Ga} being the number of Pd and Ga atoms contained in the slab. By repeating the calculation for another slab (111)X'/(-1-1-1)Pd_3 we obtain the surface free energy difference between the termination X and X' as:

$$G_{surf}^{(111)X}(\mu_{Ga}) - G_{surf}^{(111)X'}(\mu_{Ga}) \approx E_{slab}^{(111)X/(-1-1-1)Pd_3} - n_{Pd}^{(111)X/(-1-1-1)Pd_3}\mu_{Pd} - n_{Ga}^{(111)X/(-1-1-1)Pd_3}\mu_{Ga} - E_{slab}^{(111)X'/(-1-1-1)Pd_3} + n_{Pd}^{(111)X'/(-1-1-1)Pd_3}\mu_{Pd} + n_{Ga}^{(111)X'/(-1-1-1)Pd_3}\mu_{Ga}$$

Equation 2

The dependency of G_{surf} on μ_{Pd} can be dropped, since μ_{Ga} and μ_{Pd} are related by the relationship given by the chemical equilibrium between the sources and the PdGa bulk.

$$4\mu_{Ga} + 4\mu_{Pd} = \mu_{PdGa(bulk)}$$

It must be noted that the free energy of the slab should in principle be used instead of the 0K DFT total energy. However the influence of zero point vibrational effects and entropic contributions can be neglected in many cases, especially when surface energy differences are concerned.[8-10]

The same procedure was applied to obtain the surface energy differences for the (-1-1-1) termination. As reference terminations in Figure 4 we used (111)Ga_3, and (-1-1-1)Pd_3 which therefore appear constant in the respective graph.

Calculations on bulk Pd, bulk Ga (α phase) and bulk PdGa have been performed using the primitive bulk unit cells of the two systems. For all the systems considered the PWSCF package[11] was used for the calculations. The structural optimization has been performed until the largest forces on the atoms were as small as $5 \cdot 10^{-4}$ Ry/Å. We used PBE exchange-correlation functional[12], ultrasoft pseudopotential[13] for all elements and a plane wave cutoff of 30 Ryd. A convergence test was carried out using a plane wave cutoff of 40 Ryd. With respect to a 30 Ryd cutoff calculation the change in cohesive energy of PdGa gives a difference of about 1 meV/atom. K-points sampling was performed using a 3x3x1 Monkhorst pack grid for the PdGa slabs and a 4x4x4 grid for the bulks of Pd and Ga.

Figure 9 shows the typical setup for the calculation of G_{surf}: two slabs showing one similar surface are optimized.

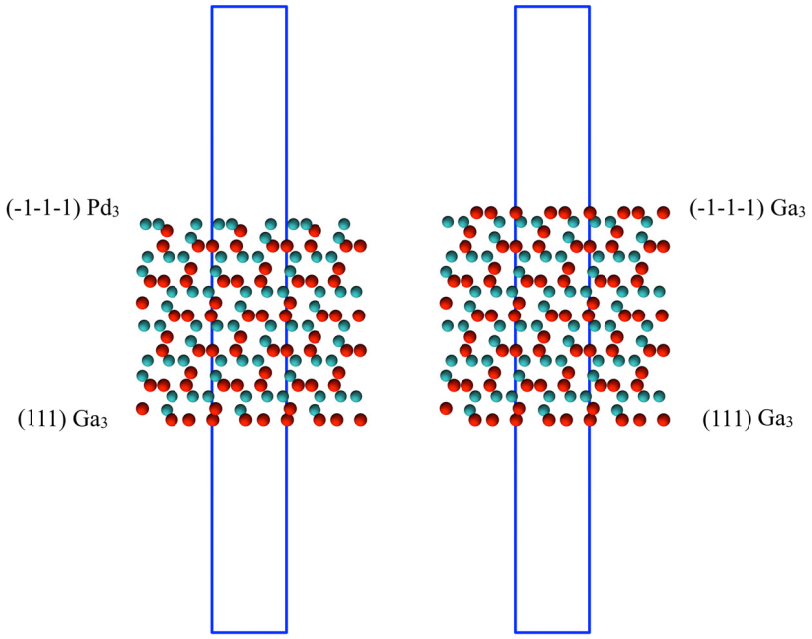

Figure 9 Lateral view of two slabs used in the calculation of the surface free energies. The lower surface (111) Ga_3 is the same in both slabs, allowing to subtract the contribution of the latter face, and to obtain the difference between the surface energies of the surfaces (-1-1-1)Pd_3 and (-1-1-1)Ga_3. Shown are also the simulation box (in blue) including a vacuum region below and above the slab, and two repetition units in the lateral direction.

3. Estimation of the chemical potential from kink energy considerations:

Because of the peculiar structure of PdGa, Pd and Ga units lack lateral interaction at the surface. This becomes clear from the comparison of in-plane and out-of-plane nearest neighbor distances (in-plane: 0.43/0.69 nm for trimer/atomic distance; out-of-plane: 0.25 nm). Hence the lateral bonding of atoms on the (111) and (-1-1-1) surfaces is weak compared to the out-of-plane bonding and consequently the energy of a surface unit does not depend on the position in the sample: adatom, kink, step, and surface sites are energetically equivalent. The energy of kink units has therefore been computed as the energy difference between slabs with a contiguous number of layers, in the two orientations.

For the estimation of chemical potentials it was assumed that the sources of Pd and Ga are in equilibrium with kink units of the crystal and that the two surfaces equilibrate independently. In this case the following set of equations holds for both orientations:

$$4\mu_{Ga} = \mu_{Ga1}^{kink} + \mu_{Ga3}^{kink}$$
$$4\mu_{Pd} = \mu_{Pd1}^{kink} + \mu_{Pd3}^{kink} \qquad \text{Equation 3}$$

where μ^{kink} is the change in energy of the system upon removal of a kink unit (which can be either a monomer or a trimer, according to the kink type). In simple crystals the kink energy has the special property of being equal to the cohesive energy. In the PdGa sample kink energies are related to the bulk energy by the relationship:

$$\mu_{Ga1}^{kink} + \mu_{Ga3}^{kink} + \mu_{Pd1}^{kink} + \mu_{Pd3}^{kink} = \mu_{PdGa(bulk)} \qquad \text{Equation 4}$$

The relationships in Equation 3 and Equation 4 hold separately for both the (111) and (-1-1-1) orientations and can be combined to recover the equilibrium condition between the bulk and the sources as expressed in the previous paragraph. Therefore the values of the surface chemical potentials given by Equation 3 and 4 are compatible with the more general conditions under which the Gibbs surface energy profiles (Equations 1 and 2) were obtained.

4. DFT vacancy simulation part:

Electronic structure calculations were performed in the framework of density functional theory (DFT) using the mixed plane wave-gaussian (GPW) basis set approach implemented in CP2K.[14] Kohn-Sham equations were solved using the PBE exchange correlation functional, Goedecker-Teter-Hutter (GTH) pseudopotentials and contracted gaussian basis sets[15] for all elements. The Poisson equation was solved by expanding the charge density in plane waves using a cutoff of 280 Rydberg. The surface unit cell of each PdGa slab is rectangular, corresponding to the $3x(2x\sqrt{3})$ primitive hexagonal surface unit cell. After the electronic optimization was carried out, the individual states have been analytically extrapolated into the vacuum region using the matching procedure described in [16] and STM images have been computed using the Tersoff-Hamann (TH) approximation, with a negative bias of 0.5 eV. It must be observed that the original TH approximation only considers tunneling from states at Fermi level; however, if the bias voltage is small compared to the work functions of the tip and the sample, the approximation can be easily modified to account for non-zero bias voltages.[17]

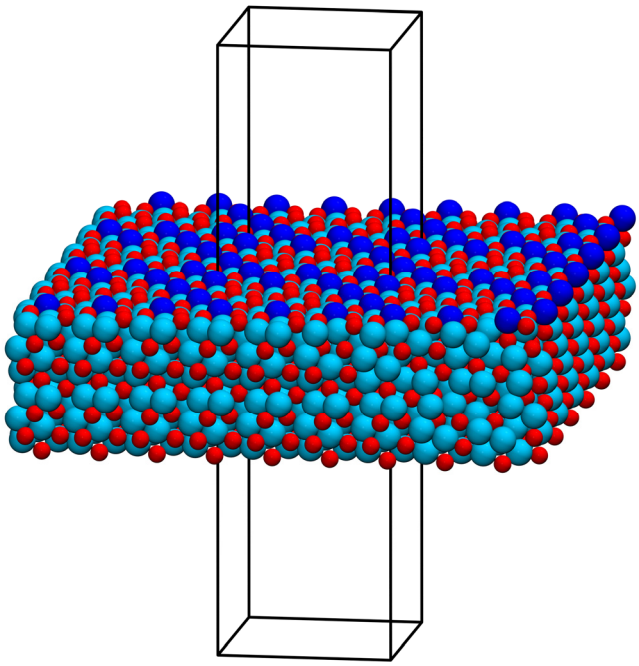

Figure 10. Perspective view of a slab used to compute the STM profile of a surface with vacancies. In this case, a Pd_1 surface is shown, with the Pd atoms at the surface highlighted in blue, to underline the presence of a 2x2 vacancy pattern. 3x3 lateral simulation cells are shown.

5. Projected density of states of the clean surfaces

For the discussed surfaces, the pDOS (based on calculations done with q-Espresso[11]) is plotted together with PdGa(bulk) and Pd(111) in Figure 11, in line with ultra-violet photoemission spectroscopy results.[18] In comparison to Pd(111) the PdGa surfaces exhibit a sharper d-band, and thus a stronger localization of electronic states. In addition, the Pd *d*-band edge of both PdGa surfaces is found at lower energies, a hint for a weaker binding of adsorbed molecules on the IMC surface, in agreement with TDS results.[18] Furthermore, the center of the Pd *d*-band shifts remarkably, depending on the distance of the projection layer from the surface as shown in Figure 11. A strong peak can be found around 2 eV below the Fermi energy for the projection on Pd *d*-bands of both PdGa surfaces which is absent in bulk PdGa. The overall shape differs only slightly for PdGa:B(111)Pd_3 and PdGa:B(-1-1-1)Pd_1, and thus the catalytic activity of the two surface terminations is expected similar by the *d*-band model.

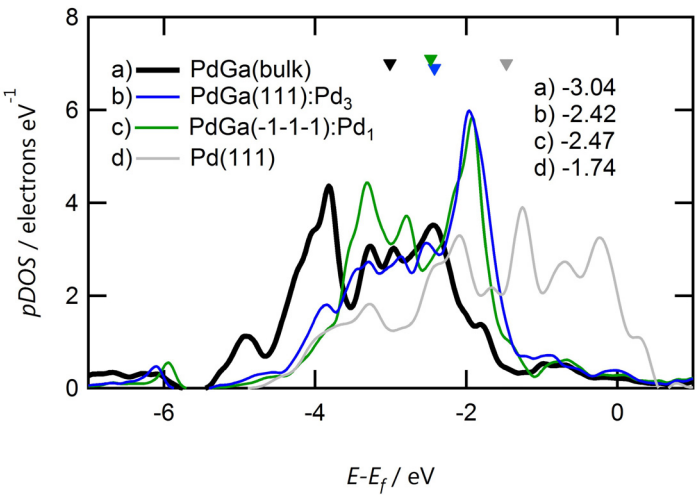

Figure 11 The pDOS of the Pd 4*d*-bands of the two studied surfaces in comparison with that of Pd(111) and PdGa(bulk). The center of the *d*-band (colored triangles in the top) is shifted towards lower energies for the PdGa surfaces with respect to Pd(111). Values of the positions of the *d*-band centers with respect to E_F are given in the top right part of the graph.

6. Hydrogen adsorption and projected density of states

In order to test the adsorption properties of the available sites on the two most stable surface terminations (PdGa:B(111)Pd_3 and PdGa:B(-1-1-1)Pd_1) we performed *ab-initio* simulations using cp2k, using similar cells as the ones described above. We choose cp2k because it allows a large supercell where adsorbed species can be considered as isolated even with boundary conditions. In order to screen a large number of molecular and atomic adsorption sites, we first adopted thin slabs with 8 layers (192 atoms) in the substrate (12 or 36 atoms per layer), then we fully optimized the best configurations using thicker slabs with 24 layers, which were also used to compute the adsorption energies. Basis set superposition error (BSSE) was verified in a specific case to amount to less than 0.02 eV, thus not affecting considerably our results.

For each case (H_2 on Pd_1, H_2 on Pd_3, H on Pd_1, H on Pd_3) we started from a grid of initial configurations. We could draw the following conclusions for the four cases:

1. H_2 on Pd_1. The best configuration is an on-top adsorption site (E_{ads}=-0.22 eV). The second best site is an on-top site on a subsurface trimer, already almost not bound.
2. H_2 on Pd_3. Also in this case, the best configuration is an on-top adsorption site (E_{ads}=-0.28 eV). The second best site is a bridge site on the trimer, less bound by 0.15 eV
3. H on Pd_1. In this case the best configuration is a hollow site on the subsurface Pd_3 trimer (E_{ads}=-0.33 eV per H couple, with respect to the molecule in gas phase). The second best site is barely bound, with an energy worse by 0.23 eV.
4. H on Pd_3. In this case the best configuration is a hollow site on the surface Pd_3 trimer (E_{ads}=-1.13 eV per H couple, with respect to the molecule in gas phase). The second best configuration, a hollow site on the same trimer, is less bound by 0.54 eV.

We show in Figure 12 the projected density of states on the *d*-bands of surface and subsurface Pd atoms, together with the projection on the H *s*-bands, upon adsorption of molecular and atomic hydrogen. As mentioned in the main text, hydrogen uptake of PdGa is not expected.[19]

A modification of the *d*-bands upon adsorption is clearly noticeable. For example, in a), we note that the on-top adsorption on the Pd_1 makes the peak at -2 eV disappear. The same happens on the Pd_3 (panel c)). But also in the case of atomic adsorption (panels b) and d)), a downward shift of the band is observed. The observation done for H adsorption on Pd(111) in [20] thus remains valid, the authors recognize that the correlation between band-center position and molecular adsorption is able to explain several observed phenomena in reactivity but that... "This analysis shows that the d-band model is only appropriate if the interaction between adsorbate and substrate is not too strong. If there is a strong coupling, then the response of the local *d*-band to the presence of the adsorbate has to be taken into account in addition to the *d*-band position in order to understand the reactivity."[19]

Additionally, we performed a Bader analysis in order to study the bonding of hydrogen atoms to the surface trimer (Pd_3 case) and to the subsurface trimer (Pd_1 case). We use the procedure described in [21]. First, the boundaries of atomic basins are determined by a zero-flux condition applied to the electronic density. Then, the atomic overlap matrix of the molecular orbitals is obtained by integration over Bader domains of a given atom. The idea is then that if two orbitals will overlap significantly in the basin of an atom A and in the basin of an atom B, this overlap will contribute to the bonding between A and B. The bond-order between two atoms A and B is then obtained by summing all such products of overlaps on basins A and B for all orbital pairs. The C-C triple bond in acetylene leads for example to a bond order of

2.885, the C-C double bond in ethylene to 1.984, the C-C single bond in ethane to 1.013, and the bond in the HF molecule to 0.480.
In our case, the adsorption to the trimer leads to a bond order of 0.48 (summed over all Pd atoms) for the Pd_1 subsurface trimer, and to a bond order of 0.52 for the Pd_3 surface timer.

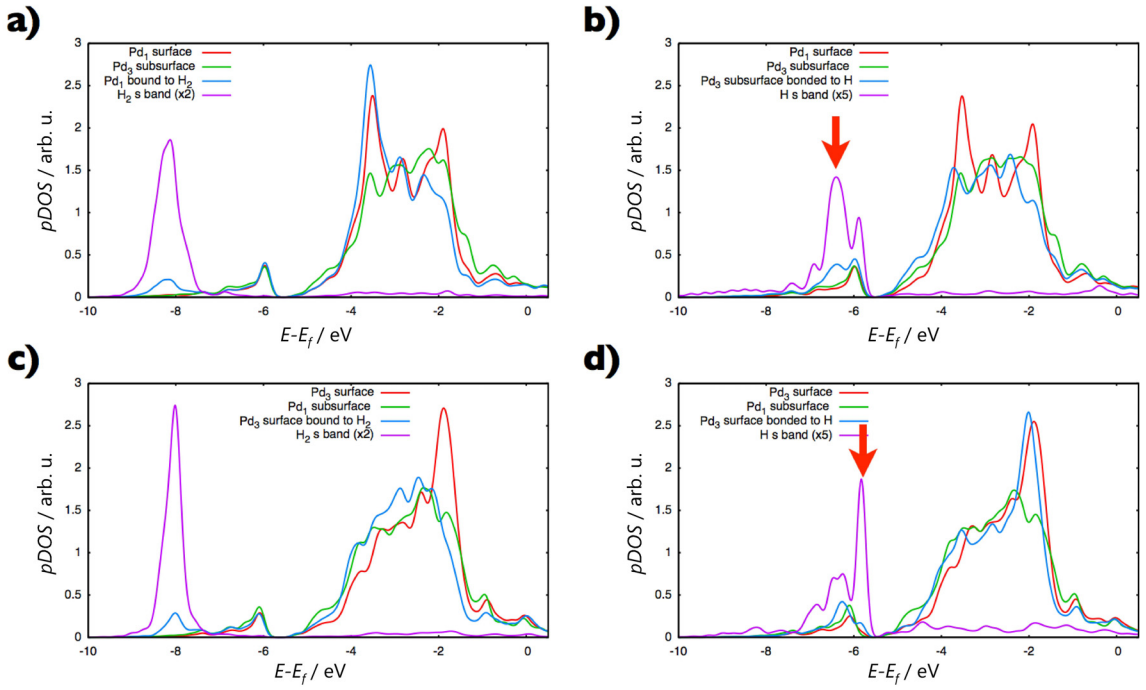

Figure 12 The DOS projected on the *d*-bands of selected Pd surface atoms and on the *s*-band of hydrogen atoms.

7. References

[1] A. Barbieri, M. A. Van Hove, private communication (http://www.ap.cityu.edu.hk/personal-website/Van-Hove.htm) ed.

[2] J. B. Pendry, *J. Phys. C: Solid State Phys.* **1980**, *13*, 937-944.

[3] P. J. Rous, J. B. Pendry, *Surf. Sci.* **1989**, *219*, 355-372.

[4] M. A. Vanhove, W. Moritz, H. Over, P. J. Rous, A. Wander, A. Barbieri, N. Materer, U. Starke, D. Jentz, J. M. Powers, G. Held, G. A. Somorjai, *Surf. Sci.* **1993**, *287*, 428-431.

[5] M. A. Van Hove, W. H. Weinberg, C. M. Chan, *Low-Energy Electron Diffraction*, Springer Verlag, Heidelberg, **1986**.

[6] V. Fiorentini, M. Methfessel, *J. Phys.: Condens. Matter* **1996**, *8*, 6525-6529.

[7] J. C. Boettger, J. R. Smith, U. Birkenheuer, N. Rosch, S. B. Trickey, J. R. Sabin, S. P. Apell, *J. Phys.: Condens. Matter* **1998**, *10*, 893-894.

[8] N. Moll, A. Kley, E. Pehlke, M. Scheffler, *Phys. Rev. B: Condens. Matter Mater. Phys.* **1996**, *54*, 8844-8855.

[9] S. Sanna, W. G. Schmidt, *Phys. Rev. B: Condens. Matter Mater. Phys.* **2010**, *81*.

[10] G. X. Qian, R. M. Martin, D. J. Chadi, *Phys. Rev. B: Condens. Matter Mater. Phys.* **1988**, *38*, 7649-7663.

[11] P. Giannozzi, S. Baroni, N. Bonini, M. Calandra, R. Car, C. Cavazzoni, D. Ceresoli, G. L. Chiarotti, M. Cococcioni, I. Dabo, A. Dal Corso, S. de Gironcoli, S. Fabris, G. Fratesi, R. Gebauer, U. Gerstmann, C. Gougoussis, A. Kokalj, M. Lazzeri, L. Martin-Samos, N. Marzari, F. Mauri, R. Mazzarello, S. Paolini, A. Pasquarello, L. Paulatto, C. Sbraccia, S. Scandolo, G. Sclauzero, A. P. Seitsonen, A. Smogunov, P. Umari, R. M. Wentzcovitch, *J. Phys.: Condens. Matter* **2009**, *21*.

[12] J. P. Perdew, K. Burke, M. Ernzerhof, *Phys. Rev. Lett.* **1996**, *77*, 3865-3868.

[13] D. Vanderbilt, *Phys. Rev. B: Condens. Matter Mater. Phys.* **1990**, *41*, 7892-7895.

[14] J. VandeVondele, M. Krack, F. Mohamed, M. Parrinello, T. Chassaing, J. Hutter, http://cp2k.berlios.de/ ed., **2005**.

[15] J. VandeVondele, J. Hutter, *J. Chem. Phys.* **2007**, *127*.

[16] M. Rohlfing, R. Temirov, F. S. Tautz, *Phys. Rev. B: Condens. Matter Mater. Phys.* **2007**, *76*.

[17] N. D. Lang, *Phys. Rev. B: Condens. Matter Mater. Phys.* **1986**, *34*, 5947-5950.

[18] D. Rosenthal, R. Widmer, R. Wagner, P. Gille, M. Armbrüster, Y. Grin, R. Schlögl, O. Gröning, *Langmuir* **2012**, *28*, 6848-6856.

[19] M. Klanjsek, A. Gradisek, A. Kocjan, M. Bobnar, P. Jeglic, M. Wencka, Z. Jaglicic, P. Popcevic, J. Ivkov, A. Smontara, P. Gille, M. Armbruster, Y. Grin, J. Dolinsek, *J. Phys.: Condens. Matter* **2012**, *24*.

[20] A. Roudgar, A. Gross, *J. Electroanal. Chem.* **2003**, *548*, 121-130.

[21] J. G. Angyan, M. Loos, I. Mayer, *J. Phys. Chem.* **1994**, *98*, 5244-5248.